

Article

# Functionalization of Magnetic Nanoparticles by Folate as Potential MRI Contrast Agent for Breast Cancer Diagnostics

Hamid Heydari Sheikh Hossein <sup>1</sup>, Iraj Jabbari <sup>2</sup>, Atefeh Zarepour <sup>1</sup>, Ali Zarrabi <sup>1,3,\*</sup>,  
Milad Ashrafizadeh <sup>4</sup>, Afrooz Taherian <sup>2</sup> and Pooyan Makvandi <sup>5,6,\*</sup>

<sup>1</sup> Department of Biotechnology, Faculty of Biological Sciences and Technology, University of Isfahan, Isfahan 81746-73441, Iran; Hamidheydari93@gmail.com (H.H.S.H.); atefeh.zarepour@gmail.com (A.Z.)

<sup>2</sup> Faculty of Physics, University of Isfahan, Isfahan 81746-73441, Iran; i\_jabbari@yahoo.com (I.J.); Afrooztaherian@gmail.com (A.T.)

<sup>3</sup> Sabanci University Nanotechnology Research and Application Center (SUNUM), Tuzla, 34956 Istanbul, Turkey

<sup>4</sup> Department of Basic Sciences, Faculty of Veterinary Medicine, University of Tabriz, Tabriz 51666-16471, Iran; dvm.milad73@yahoo.com

<sup>5</sup> Istituto Italiano di Tecnologia, Centre for Micro-BioRobotics, viale Rinaldo Piaggio 34, 56025 Pontedera, Pisa, Italy

<sup>6</sup> Department of Medical Nanotechnology, Faculty of Advanced, Technologies in Medicine, Iran University of Medical Sciences, Tehran 14496-14535, Iran

\* Correspondence: alizarrabi@sabanciuniv.edu (A.Z.); pooyanmakvandi@gmail.com (P.M.)

Academic Editors: Zoltan Kovacs and Gyula Tircsó

Received: 8 July 2020; Accepted: 3 September 2020; Published: 4 September 2020



**Abstract:** In recent years, the intrinsic magnetic properties of magnetic nanoparticles (MNPs) have made them one of the most promising candidates for magnetic resonance imaging (MRI). This study aims to evaluate the effect of different coating agents (with and without targeting agents) on the magnetic property of MNPs. In detail, iron oxide nanoparticles (IONPs) were prepared by the polyol method. The nanoparticles were then divided into two groups, one of which was coated with silica (SiO<sub>2</sub>) and hyperbranched polyglycerol (HPG) (SPION@SiO<sub>2</sub>@HPG); the other was covered by HPG alone (SPION@HPG). In the following section, folic acid (FA), as a targeting agent, was attached on the surface of nanoparticles. Physicochemical properties of nanostructures were characterized using Fourier transform infrared spectroscopy (FT-IR), transmission electron microscopy (TEM), and a vibrating sample magnetometer (VSM). TEM results showed that SPION@HPG was monodispersed with the average size of about 20 nm, while SPION@SiO<sub>2</sub>@HPG had a size of about 25 nm. Moreover, HPG coated nanoparticles had much lower magnetic saturation than the silica coated ones. The MR signal intensity of the nanostructures showed a relation between increasing the nanoparticle concentrations inside the MCF-7 cells and decreasing the signal related to the T<sub>2</sub> relaxation time. The comparison of coating showed that SPION@SiO<sub>2</sub>@HPG (with/without a targeting agent) had significantly higher r<sub>2</sub> value in comparison to Fe<sub>3</sub>O<sub>4</sub>@HPG. Based on the results of this study, the Fe<sub>3</sub>O<sub>4</sub>@SiO<sub>2</sub>@HPG-FA nanoparticles have shown the best magnetic properties, and can be considered promising contrast agents for magnetic resonance imaging applications.

**Keywords:** contrast agents; MRI; polyglycerol; silica nanoparticles; SPION

## 1. Introduction

Because of their unique physicochemical properties, nanoparticles (NP) have broad applications in a variety of biomedical researches, like implants [1], drug delivery systems [2], tissue engineering [3],

and infection therapy [4]. One of the significant applications of nanomaterials in medicine is the timely detection and treatment of cancer [5]. Different nanoprobe such as quantum dots have been developed for the early diagnosis of breast cancer, and this requires understanding the distribution and removal of nanoparticles at the breast tumor site [6]. One of the potential applications of NP is in diagnostic medicine, particularly for magnetic resonance imaging (MRI).

Briefly, MRI is a noninvasive imaging modality that, by exposing the hydrogen protons to an external magnetic field ( $B_0$ ), leads to aligning some parts of protons towards  $B_0$  direction and then rotation around it. Then, radiofrequency (RF) waves apply in the equal frequency with the precession of the protons, resulting in the RF pulse energy adding to the protons. Subsequently, when the RF pulse is turned off, protons flip back to the original state and generate a radiofrequency signal in a process called “relaxation” [7–9].

Two kinds of relaxation processes exist; namely, longitudinal or  $T_1$  relaxation, also called spin-lattice relaxation, and transverse or  $T_2$  relaxation, referred to as spin-spin relaxation. The former refers to the process through which the net longitudinal magnetization goes back to its earliest maximum value parallel to the magnetic field, as described in the following equation [8]:

$$M_z = M_{z,0} \left( 1 - e^{-\frac{t}{T_1}} \right) \quad (1)$$

where  $M_{z,0}$  refers to the magnetization in an equilibrium state, and  $T_1$  stands for the time for  $M_z$  to reach 63% of the original magnetization after the application of the RF pulse.

The latter is the process referring to the transverse components of magnetization decay or dephases, as described in the following equation [8]:

$$M_{xy} = M_{xy,0} e^{-\frac{t}{T_2}} \quad (2)$$

in which  $M_{xy}$  illustrates the decay of magnetization,  $M_{xy,0}$  depicts the initial transverse magnetization, and  $T_2$  shows the time for transversal magnetization dropping to 37%.

Although MRI has gained much publicity in medicine diagnostics, there are some drawbacks associated with it. One of the most important ones is low sensitivity that reduces its potential in molecular level detection [10]. To overcome this restriction, increasing contrast between healthy and diseased tissues is of great importance.

Typically, elements like gadolinium, iron, and manganese that possess unpaired electron spins are referred to as  $T_1$  contrast agents. They could increase the  $T_1$  relaxation time via increasing the signal intensity, thus causing a positive contrast in images. On the other hand, superparamagnetic iron oxide nanoparticles (SPIONs) decrease the signal intensity via the reduction of  $T_2$  relaxation time, resulting in images with negative contrast [11–14]. Gadolinium is the most widely used contrast agent in MRI, which has many limitations, the most important of which are its cytotoxicity and non-biodegradability. Recently, SPIONs have attracted more attention due to their effectiveness at low concentration, biocompatibility, and easy functionalization that make them suitable alternatives for gadolinium in MRI [15,16].

Apart from their use as MRI contrast agents, iron oxide nanoparticles have several other potential applications, like drug delivery vehicle, cell tracking, tissue engineering, separation of biomolecules, and immobilization of enzymes or proteins in biomedical engineering [17]. However, there are obstacles and challenges for using SPIONs, including their tendency to aggregation and the protein corona effect [10–12,14]. One of the most prevalent approaches used to meet these obstacles is coating the surface of nanoparticles with polymers [18,19].

Hyperbranched polyglycerol (HPG) is an amphiphilic biocompatible polyether polyol with a high degree of branching, a dense structure, and a large number of terminal hydroxyl groups which can provide a broad area for encapsulation of different types of drugs and attachment of targeting molecules. Coating the nanoparticles with HPG provides them with suitable properties, such as

increasing their water solubility, biocompatibility, and protein resistance ability, which are comparable to polyethylene glycol (PEG) [20,21]. Moreover, HPG polymers possess high thermal and oxidative stability [22,23].

One of the drawbacks of nanocarriers is their cytotoxicity against normal cells. This problem can be overcome using biocompatible polymers [24,25]. Furthermore, coating nanoparticles can delay their clearing from the body, and improve stability [26]. Silica is extensively used for coating nanoparticles to, in one hand, prevent their aggregation, and on the other hand, support against oxidation. It is held that silica can promote the biocompatibility of nanoparticles. The interesting point is that silica has a high affinity for binding into surface of nanoparticles [27]. The recently published articles have also confirmed the aforementioned statements, and benefits of using silica for coating nanoparticles [28].

In this research, the impact of different coatings on the  $r_2$  relaxivity of MR imaging of iron oxide nanoparticles was investigated. For this purpose, iron oxide magnetic nanoparticles were synthesized using the polyol method. Next, for a comparison of coating effects, synthesized nanoparticles were coated with HPG and SiO<sub>2</sub>-HPG. Then, folic acid as targeting ligand was conjugated in a covalent bond to the terminal hydroxyl groups of coating nanoparticles. Different types of physicochemical analyses (like Fourier transform infrared spectroscopy (FT-IR), transmission electron microscopy (TEM), and vibrating sample magnetometer (VSM)) were used for the characterization of the nanoparticles. Moreover, the cytotoxicity of nanoparticles was determined using MTT colorimetric assay. Finally, the differences between the magnetic properties of the coated nanoparticles (with/without targeting agent) were investigated via MRI analysis.

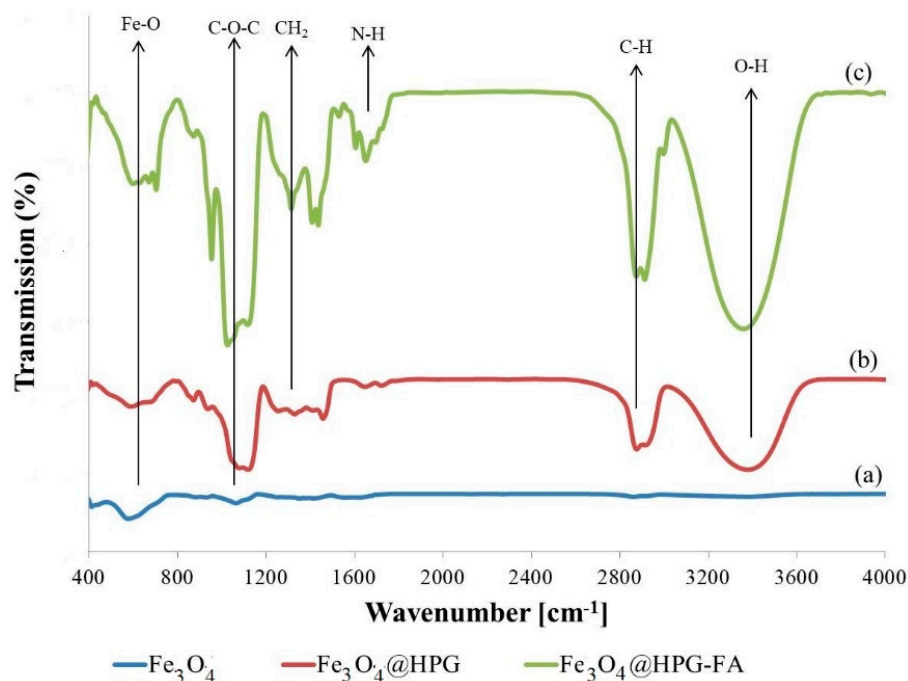
## 2. Results

### 2.1. Synthesis and Characterization of Nanoparticles

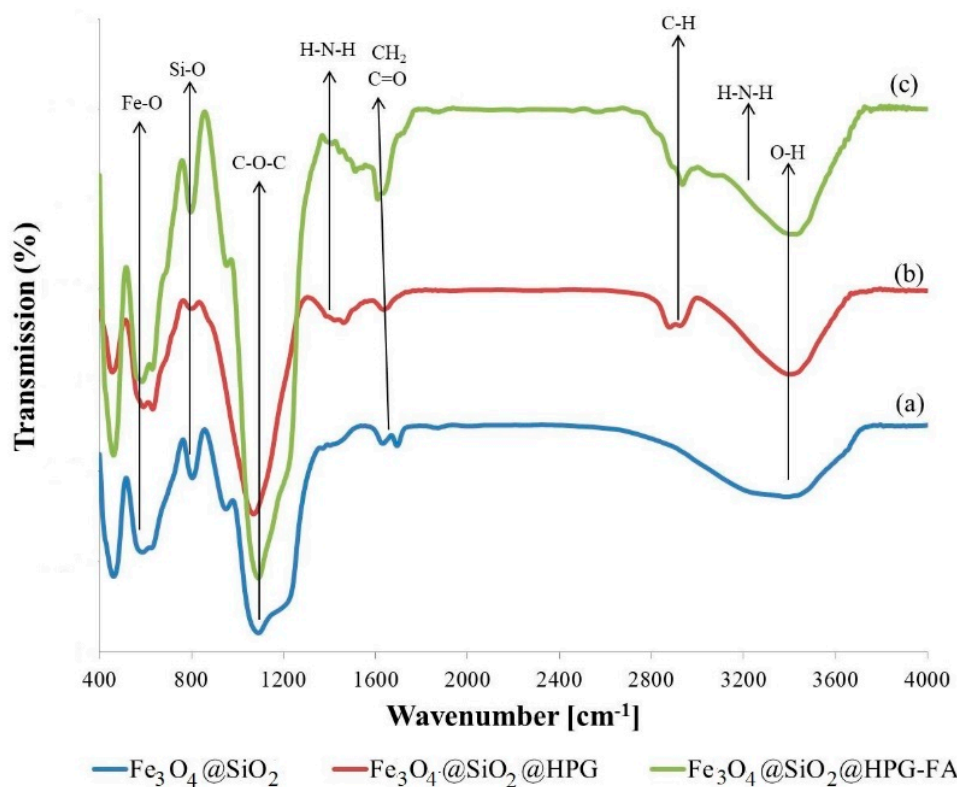
Fe<sub>3</sub>O<sub>4</sub> nanoparticles were synthesized with success by using the polyol method, and then they were coated with SiO<sub>2</sub> and HPG. The changes that occurred in the chemical structure of the nanoparticles were characterized by FT-IR spectroscopy (Figures 1 and 2). Based on the result in Figure 1, the absorption peak at about 585 cm<sup>-1</sup> belongs to the stretching vibration of Fe-O bonds in Fe<sub>3</sub>O<sub>4</sub> nanoparticles, which could confirm the presence of Fe as the essential element in the nanoparticles. The characteristic band at around 1115–1050 cm<sup>-1</sup> is associated with the C-O-C stretching, which could also reveal the conjugation of TREGs as an organic component on the particles surface (Figure 1a) [29–31].

Figure 1b illustrates the FTIR spectrum of nanoparticles coated by hyperbranched polyglycerol. The broad band at 3400 cm<sup>-1</sup> is associated with the stretching vibration of the O-H bond, and the split peaks between 2800–2900 cm<sup>-1</sup> belong to the C-H stretching (symmetric and asymmetric) of the polyglycerol. Moreover, the bands at around 1300–1500 cm<sup>-1</sup> are associated with the bending vibration of the CH<sub>2</sub> Groups. These results approve the polymerization of monomers on the surface of nanoparticles [16,21,30,32].

Figure 1c shows the FTIR result of Fe<sub>3</sub>O<sub>4</sub>@HPG-FA nanoparticles. The intense peaks at 1400 and 1650 cm<sup>-1</sup> correspond to the p-amino benzoic acid moieties and aromatic ring stretch of FA pteridine ring. Furthermore, significant broadening peaks at 1620 cm<sup>-1</sup> and 1650 cm<sup>-1</sup> represent the N-H groups of FA components, confirming the emergence of targeted SPION@HPG with FA [33,34].



**Figure 1.** FT-IR spectroscopy of (a)  $\text{Fe}_3\text{O}_4$  (b) hyperbranched polyglycerol (HPG) grafted  $\text{Fe}_3\text{O}_4$  and (c)  $\text{Fe}_3\text{O}_4$ @HPG-FA.



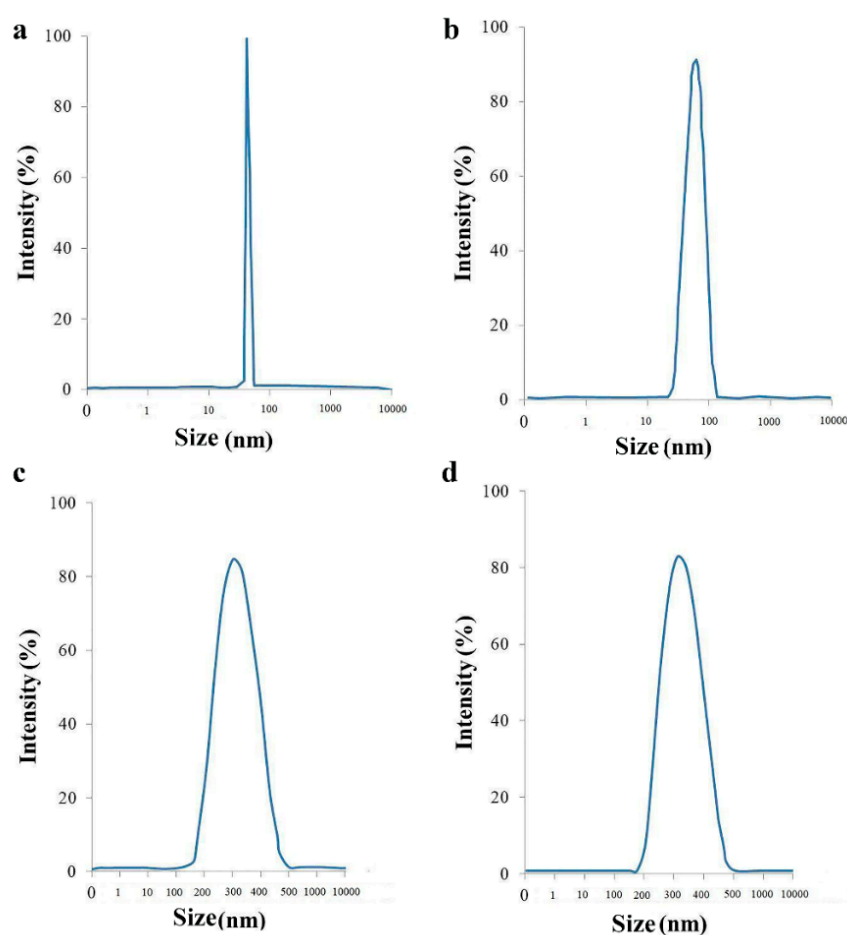
**Figure 2.** FT-IR spectroscopy of (a)  $\text{Fe}_3\text{O}_4$ @ $\text{SiO}_2$ , (b)  $\text{Fe}_3\text{O}_4$ @ $\text{SiO}_2$ @HPG, and (c)  $\text{Fe}_3\text{O}_4$ @ $\text{SiO}_2$ @HPG-FA.

In Figure 2a, the band at around  $590\text{ cm}^{-1}$  is attributed to the vibration of the Fe-O bond, which shows the presence of  $\text{Fe}_3\text{O}_4$  components. In addition, the bands at about  $1089\text{ cm}^{-1}$  and  $806\text{ cm}^{-1}$  are associated with the Si-O vibration, revealing the presence of the  $\text{SiO}_2$  shell. As depicted in Figure 2b, the absorbance peaks at around  $3435\text{ cm}^{-1}$  and  $1080\text{ cm}^{-1}$  confirm the presence of HPG on

the surface of nanoparticles, and they are attributed to the OH bond and C-O-C ether stretch bond, respectively [20,35].

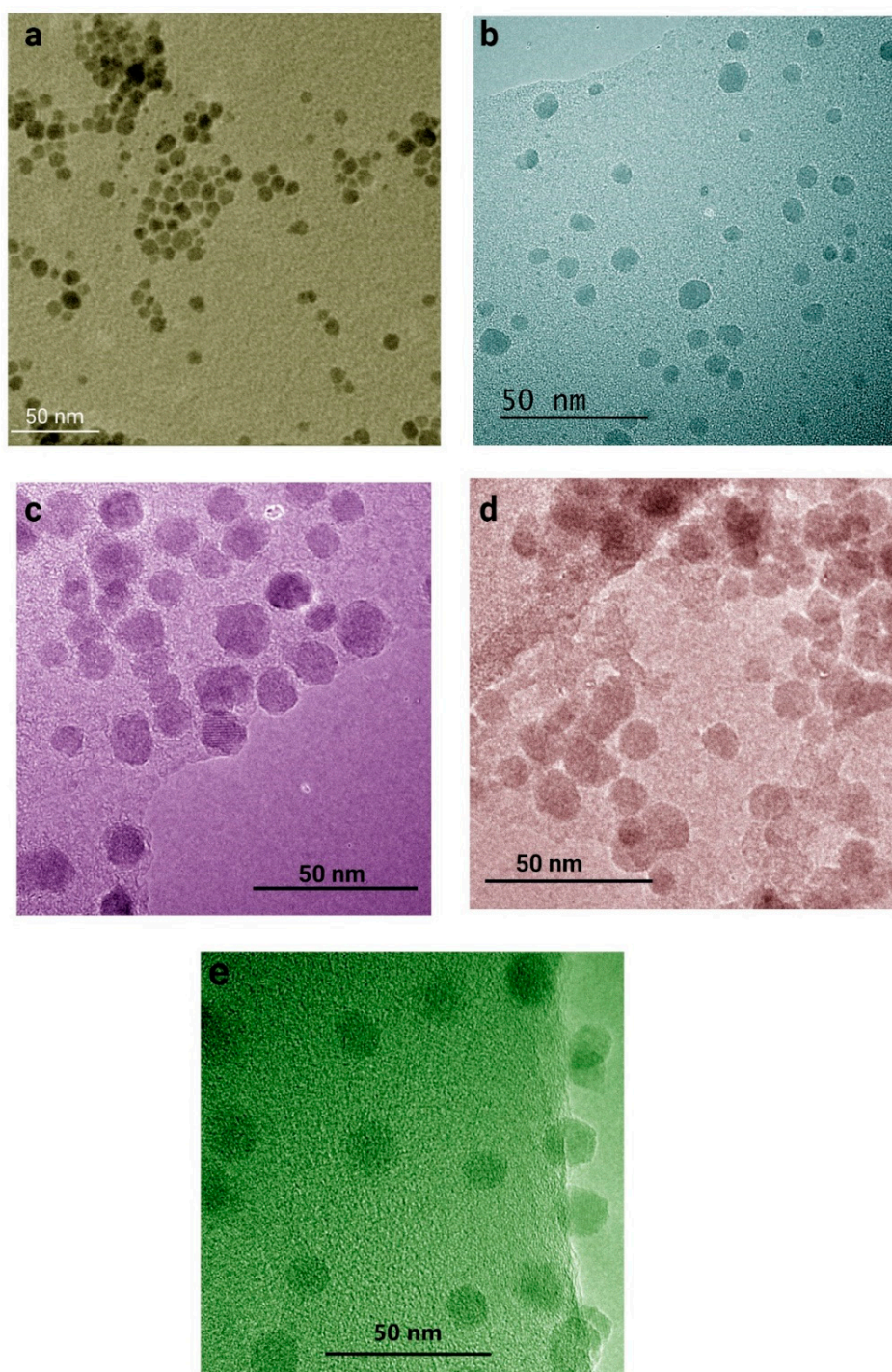
The FTIR spectra of the FA grafted  $\text{Fe}_3\text{O}_4@SiO_2@HPG$  nanoparticles illustrate peaks at  $1610$  and  $1410\text{ cm}^{-1}$ , which correspond to the aromatic ring stretch of pteridine ring and p-amino benzoic acid moieties of FA (Figure 2c). A significant broadening peak at  $1610\text{ cm}^{-1}$  also corresponds to the ester linkage that is formed between folic acid and the hydroxyl groups. Moreover, the strong band at around  $2912\text{ cm}^{-1}$  corresponds to the  $\text{CH}_2$  stretching vibrations [34,36,37].

Figure 3 shows the results of DLS analysis of synthesized and functionalized iron oxide nanoparticles after each step of surface modification. It can be seen that the synthesized  $\text{Fe}_3\text{O}_4$  nanoparticles have a narrow size distribution with a mean of  $\sim 55\text{ nm}$ , whereas after each step of functionalization, the size increased due to the presence of new layers. In agreement with the literature, the size of the modified iron oxide is increased due to the fact that coating bring new layers to the surface of magnetic nanoparticles; accordingly, the size is enhanced [38,39].



**Figure 3.** Size distribution analysis of (a)  $\text{Fe}_3\text{O}_4$ , (b)  $\text{Fe}_3\text{O}_4@HPG$ , (c)  $\text{Fe}_3\text{O}_4@SiO_2$ , and (d)  $\text{Fe}_3\text{O}_4@SiO_2@HPG$ .

The size and core-shell structure of nanoparticles were characterized by ultra-high-resolution transmission electron microscopy. For this test,  $\text{Fe}_3\text{O}_4$ ,  $\text{Fe}_3\text{O}_4@HPG$ ,  $\text{Fe}_3\text{O}_4@SiO_2$ ,  $\text{Fe}_3\text{O}_4@SiO_2@HPG$ , and  $\text{Fe}_3\text{O}_4@SiO_2@HPG\text{-FA}$  were characterized by TEM, as the results show in (Figure 4). In agreement with other literature studies [40,41], there is a difference between DLS and TEM sizes measurements which are normally attributed to the fundamental difference between intensity and number-weighted particle size distributions, and the differences between the dry and hydrodynamic radius of particles.



**Figure 4.** UHR-TEM analysis of (a)  $\text{Fe}_3\text{O}_4$ , (b)  $\text{Fe}_3\text{O}_4\text{@HPG}$ , (c)  $\text{Fe}_3\text{O}_4\text{@SiO}_2$ , (d)  $\text{Fe}_3\text{O}_4\text{@SiO}_2\text{@HPG}$ , and (e)  $\text{Fe}_3\text{O}_4\text{@SiO}_2\text{@HPG-FA}$ .

As is evident from TEM images,  $\text{Fe}_3\text{O}_4$  nanoparticles (Figure 4a) have a spherical shape with a particle size of about 10 nm. Since the HPG cannot be observed in the TEM images, the size of HPG-grafted  $\text{Fe}_3\text{O}_4$  nanoparticles is the same as that of bare nanoparticles. However, it could be seen that HPG coating positively affects the distribution of nanoparticles (Figure 4b). The  $\text{Fe}_3\text{O}_4\text{@SiO}_2$  nanoparticles show a distinct core-shell structure, and the size that is deduced from the TEM image (Figure 4c) is around 20 nm, which is smaller than  $\text{Fe}_3\text{O}_4\text{@SiO}_2\text{@HPG}$ , with a size about 30 nm. From

TEM results, we can reach the conclusion that the HPG coating conceals one core of  $\text{Fe}_3\text{O}_4$ , while several  $\text{Fe}_3\text{O}_4$  cores are covered by silica coating, which leads to the formation of semi-composite structures.

It has been reported that polyglycerol can prevent the aggregation and enhance the stability of iron oxide nanoparticles, since these coatings have high hydrophilicity. Such stability (e.g., stabilizing the nanoparticles for about 2 months) has been shown in previous literature [38,39].

## 2.2. MTT Assay

One of the most common tests used for the assessment of the impact of foreign materials on the viability of cells is MTT assay, which is based on the enzymatic reduction of MTT salt to the purple formazan brought about by the mitochondria of viable cells [33,42]. In this research, the impact of cytotoxicity of various concentrations of nanoparticles on the viability of the MCF-7 cell line was evaluated by MTT assay for two days, and the results of this test are shown in Figure 5. As is clear in the figures, both of the polymeric coated nanoparticles (with or without folic acid) have no significant effect on the viability of the cells. Moreover, the viability of cells exposed by the targeted samples was a little higher than the non-targeted ones. These results confirm the cytocompatibility of this carrier, which is a critical factor for utilizing the nanocarriers in vivo. Based on the literature, this feature is due to the presence of polyglycerol, which could provide high biocompatibility for nano drug delivery systems [43,44].

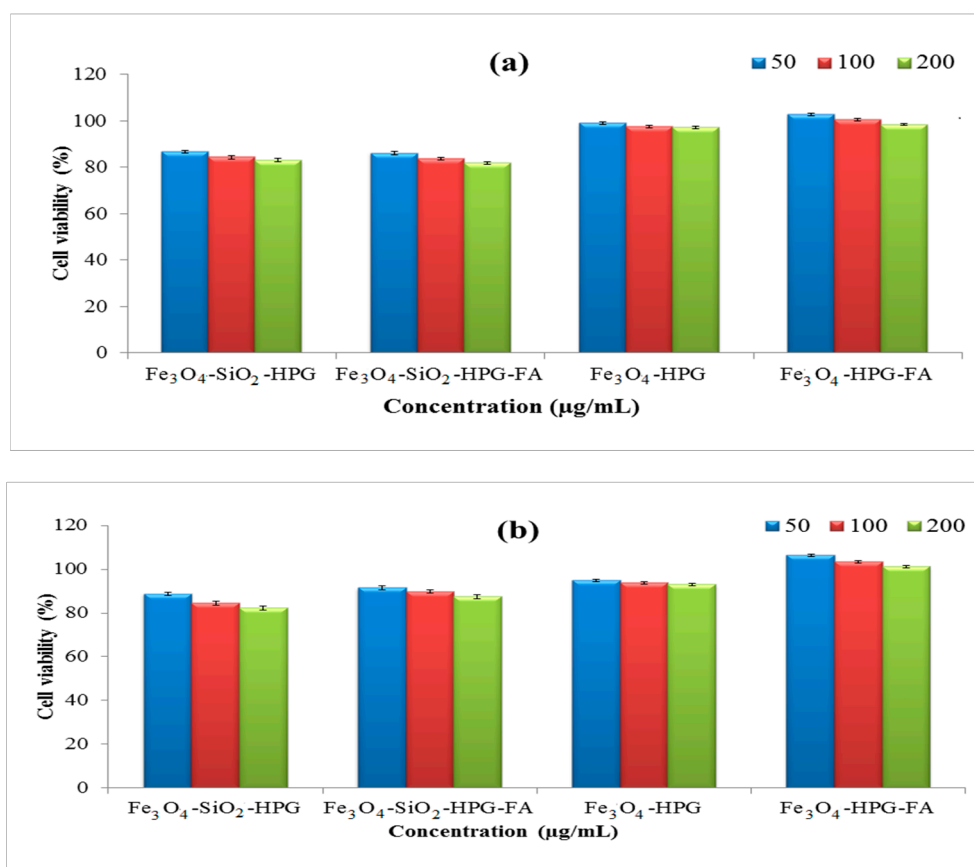


**Figure 5.** Cytotoxicity evaluation of nanoparticles after (a) 24 h and (b) 48 h on the MCF-7 cell line.

## 2.3. Value Stream Mapping (VSM)

The magnetic properties of  $\text{Fe}_3\text{O}_4$ ,  $\text{Fe}_3\text{O}_4\text{@HPG}$ ,  $\text{Fe}_3\text{O}_4\text{@HPG-FA}$ ,  $\text{Fe}_3\text{O}_4\text{@SiO}_2\text{@HPG}$ , and  $\text{Fe}_3\text{O}_4\text{@SiO}_2\text{@HPG-FA}$  were measured at room temperature by employing VSM (Figure 6). As can be seen, all magnetization curves are s-shaped over the applied magnetic field, confirming that they

all have superparamagnetic behavior. The saturation magnetization ( $M_s$ ) of  $\text{Fe}_3\text{O}_4$  nanoparticles was decreased from 64.84 to 33.86, 25.80, 10.77, and 1.66  $\text{emu/g}^{-1}$ , when  $\text{SiO}_2$ @HPG,  $\text{SiO}_2$ @HPG-FA, HPG, and HPG-FA were grafted to them [16,45]. These results reveal that HPG coating could decrease  $M_s$  of nanoparticles more than  $\text{SiO}_2$ @HPG coating, which may be due to its longer polymerization time leading to the production of a much thick layer on the surface of magnetic nanoparticles. By combining the results of VSM with TEM results, it could be said that  $\text{Fe}_3\text{O}_4$ @HPG nanoparticles contain one core of magnetic nanoparticle covered by a layer of branched polyglycerol. In contrast,  $\text{Fe}_3\text{O}_4$ @ $\text{SiO}_2$ @HPG nanoparticles are composed of a composite of some magnetic nanoparticles dispersed in the  $\text{SiO}_2$  matrix and then covered by HPG. This event also could affect the magnetization property of the nanoparticles, leading to a reduction in the amount of magnetic saturation.  $M_s$  of about 7–22  $\text{emu/g}^{-1}$  is usually adapted for biomedical and bioengineering applications; therefore, the  $\text{Fe}_3\text{O}_4$ @ $\text{SiO}_2$ @HPG nanoparticles with higher  $M_s$  are acceptable for bio applications.

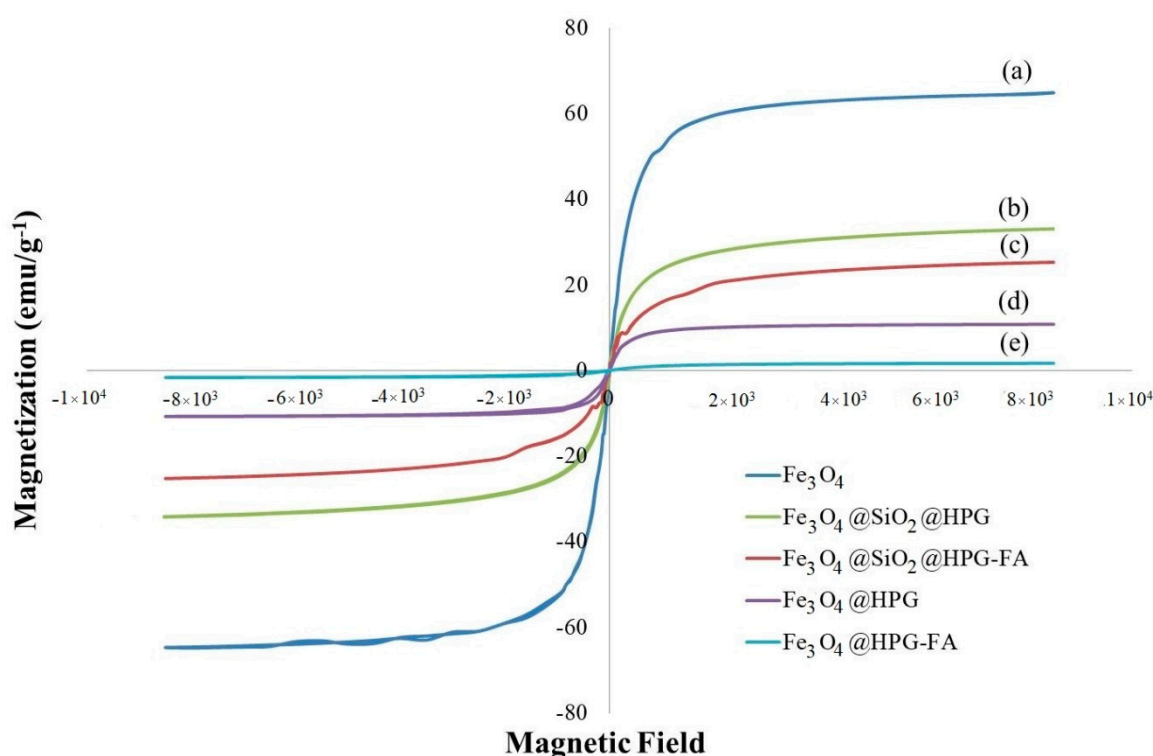


**Figure 6.** Magnetic behavior of (a)  $\text{Fe}_3\text{O}_4$  nanoparticles (b)  $\text{Fe}_3\text{O}_4$ @ $\text{SiO}_2$ @HPG (c)  $\text{Fe}_3\text{O}_4$ @ $\text{SiO}_2$ @HPG-FA (d)  $\text{Fe}_3\text{O}_4$ @HPG (e)  $\text{Fe}_3\text{O}_4$ @HPG-FA.

#### 2.4. MR Imaging of Cells after They Are Incubated by Nanoparticles

The MRI was employed in order to evaluate the impact of coating on magnetic behavior of the nanoparticles used as contrast agent. For this test,  $\text{Fe}_3\text{O}_4$ @ $\text{SiO}_2$ @HPG and  $\text{Fe}_3\text{O}_4$ @HPG with and without FA were used, and the results are described in Figure 7. According to this Figure, the MR signal intensity of the nanoparticles had a relationship with different concentrations of samples, so that by increasing the concentrations of nanoparticles inside the MCF-7 cells, the MR signal that is associated with the  $T_2$  relaxation time is significantly decreased, leading to a negative contrast in  $T_2$ -weighted images.

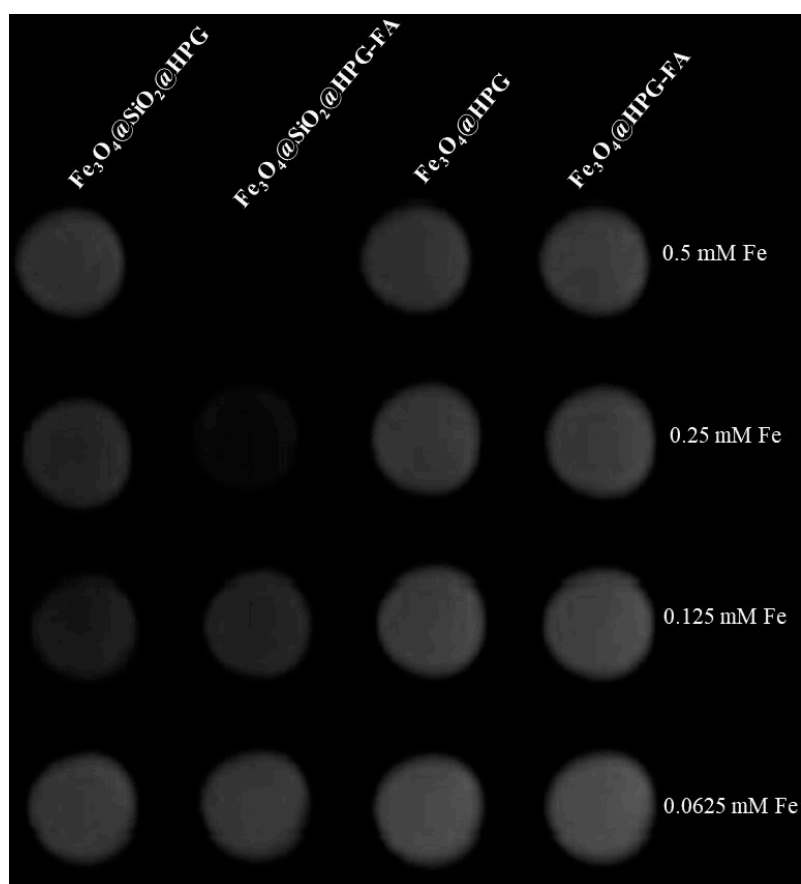


**Figure 7.**  $T_2$ -weighted image of MCF-7 cells after they are treated with different concentrations Fe of each contrast agent.

The results revealed that due to their low magnetic saturation, HPG coated nanoparticles have low amounts of  $1/T_2$  (0.5 and 0.7 for nanoparticles without and with FA, respectively), and are not suitable for MRI contrast agents (Figure 8a); while, by changing the coating of nanoparticles, the amounts of  $1/T_2$  also changed, so that it increased from  $4 \text{ S}^{-1}$  for  $\text{Fe}_3\text{O}_4@SiO_2@HPG$  to  $12 \text{ S}^{-1}$  for  $\text{Fe}_3\text{O}_4@SiO_2@HPG-FA$  (Figure 8b). Generally,  $T_2$  measurement of the samples indicated that the relaxation times ( $1/T_2$ ) increased much faster for nanoparticles targeted with folic acid than for those not targeted.

The results of  $r_2$  of different nanoparticles are listed in Table 1. Based on the results in Table 1,  $SiO_2@HPG$  coated nanoparticles have higher  $r_2$  in contrast to HPG one. Moreover, targeted samples have significantly higher  $r_2$  values in comparison to non-targeted ones due to the presence of high amounts of folate receptors on the surface of the MCF-7 cell line. When FA conjugated to  $\text{Fe}_3\text{O}_4@SiO_2@HPG$ , the  $r_2$  value was increased from  $8.87$  to  $23.25 \text{ mM}^{-1}\text{S}^{-1}$  that confirmed the targeting role of FA. The results reveal a preferential uptake of  $\text{Fe}_3\text{O}_4@SiO_2@HPG-FA$  nanoparticles by the cells overexpressing the folate receptor [46,47]. Furthermore,  $\text{Fe}_3\text{O}_4@SiO_2@HPG-FA$  targeted nanoparticles have  $r_2$   $23.25 \text{ mM}^{-1}\text{S}^{-1}$ , which is higher than  $\text{Fe}_3\text{O}_4@HPG-FA$  with  $r_2$   $0.131 \text{ mM}^{-1}\text{S}^{-1}$ . This is related to the higher  $M_s$  of these nanoparticles in comparison to the  $\text{Fe}_3\text{O}_4@HPG-FA$ , and is associated with the high amounts of HPG coating on the  $\text{Fe}_3\text{O}_4@HPG$  surface, resulting in the reduction in the magnetic intensity of nanoparticles.

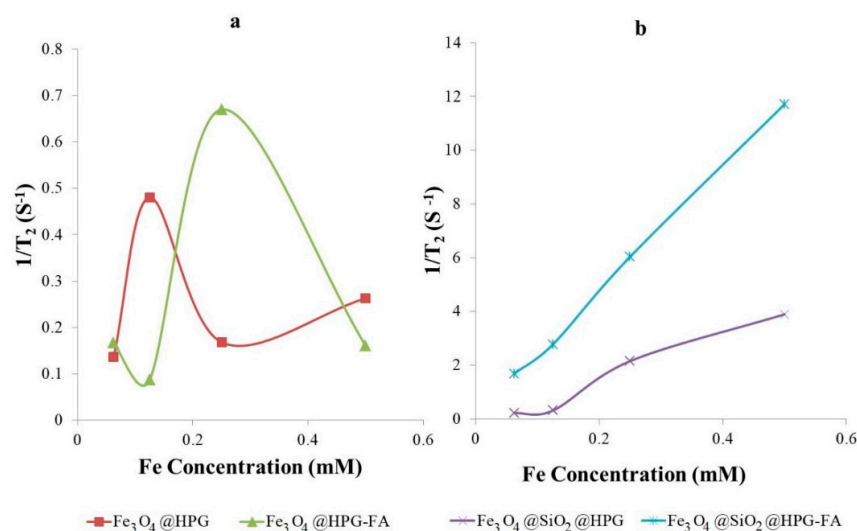


**Figure 8.**  $1/T_2$  values as a function of concentration of (a)  $Fe_3O_4@HPG$  and  $Fe_3O_4@HPG-FA$ ; (b)  $Fe_3O_4@SiO_2@HPG$  and  $Fe_3O_4@SiO_2@HPG-FA$ .

**Table 1.** In vitro Transverse relaxivities ( $r_2$ ) of MRI contrast agents.

	$r_2$ [ $mM^{-1}S^{-1}$ ]
$Fe_3O_4@SiO_2@HPG$	8.87
$Fe_3O_4@SiO_2@HPG-FA$	23.25
$Fe_3O_4@HPG$	0.029
$Fe_3O_4@HPG-FA$	0.131

### 3. Discussion

Early detection is a critical factor for successful cancer therapy. In this regard, there are several methods for the early detection of cancer, among the most important of which is MRI, a highly sensitive method with low side effects. Since the possible side effects of the high magnetic field in MRI are still unknown, the clinical application of MRI with magnetic field less than 7T is FDA approved. Therefore, it is necessary to use a contrast agent, which could increase the sensitivity of MRI detection [10]. The unique properties of magnetic nanoparticles such as excellent biocompatibility and high magnetic behavior introduce them as an appropriate candidate for biomedical applications [48]. Consequently, the design and fabrication of biocompatible water-soluble iron oxide nanoparticles to be used as contrast agents have attracted a lot of attention, and significant attempts have been made in this field [49–51]. This study mainly aimed to compare the impact of two different coatings on the magnetic property of iron oxide nanoparticles using an MRI contrast agent.

Iron oxide magnetic nanoparticles were synthesized by using the polyol method. Then, the nanoparticles were coated with  $SiO_2$  and HPG, and folic acid as a targeting ligand was conjugated to the terminal hydroxyl groups of coating nanoparticles in a covalent manner. The findings of this study showed that coating  $Fe_3O_4$  nanoparticles with  $SiO_2$  and HPG did not affect the viability of the MCF-7 cell line; while targeted nanoparticles, especially for the  $Fe_3O_4@HPG@FA$ , showed a partial cytotoxicity effect on the cells at high concentrations. This result has also been observed by other researchers [52]. The magnetic saturation was found at 33.86, 25.80, 10.77, and 1.66  $emu/g^{-1}$  when  $HPG@SiO_2$ ,  $HPG@SiO_2@HPG-FA$ , HPG, and HGP-FA were grafted to  $Fe_3O_4$  nanoparticles, which were less than that of pure nanoparticles, with  $M_s$  of about 64.84  $emu/g^{-1}$ . These differences suggest that HPG coating could decrease  $M_s$  of nanoparticles more than  $SiO_2@HPG$ . In addition, the reduction of nanoparticles' magnetization due to the surface modifications has been confirmed by several studies [53,54].

Coating nanoparticles by HPG and SiO<sub>2</sub>@HPG produced an  $r_2$  value of 0.029 and 8.87 mM<sup>-1</sup>S<sup>-1</sup>, respectively. These results demonstrated that coating nanoparticles with HPG significantly decreased the magnetic intensity of nanoparticles, due to the high polymerization and fewer number of Fe<sub>3</sub>O<sub>4</sub> in the core in comparison to the silica coating nanoparticles. These results indicate that changing the surface coatings of nanoparticles could influence the transversal relaxivities ( $r_2$ ) [38]. That the relaxivity is a vital parameter for the estimation of the efficiency of a  $T_2$  contrast agent is quite well known. Hajesmaelzadeh et al. reported that, by increasing the thickness of coating on iron oxide nanoparticles, there was an increase in their relaxivity. Moreover, they showed that with an increase in the nanoparticles size, the amount of  $r_2$  relaxivity decreased. This result confirms that the type and amount of the coating affect the  $r_2$  values relaxivities [55]. According to Bitar et al., biocompatible SiO<sub>2</sub> coating of nanoparticles makes them more dispersible in bio-media and easy to be functionalized using biomolecules for biomedicine research, too [56].

Furthermore, targeting the nanoparticles has an essential function in improving the particles selectivity against cancer cells. In addition, it could increase the accumulation of contrast agents needed for imaging in the targeted site [57]. The findings of this research reveal that the functionalization of HPG with FA leads to the attachment of nanoparticles to the folate receptors, which are expressed on the surface of MCF-7 cells that are later taken into the cell via receptor-mediated endocytosis (Figure 9). Nanoparticles lacking FA enter the MCF-7 cells using the non-specific penetration process. As a consequence, folic acid targeted nanoparticles have substantial  $r_2$  relaxivities in comparison to the non-targeted one, just as what was reported in other studies [58,59]. As was predicted, Fe<sub>3</sub>O<sub>4</sub>@SiO<sub>2</sub>@HPG-FA nanoparticles, due to their higher magnetic intensity, have better  $r_2$  relaxivities (23.25 mM<sup>-1</sup>S<sup>-1</sup>) in contrast to the Fe<sub>3</sub>O<sub>4</sub>@HPG targeted nanoparticles. Gholibegloo et al. reported that folic acid decorated magnetic nanoparticles have an  $r_2$  value of about 54 mM<sup>-1</sup>S<sup>-1</sup> [60]. However, they used cyclodextrin for the surface modification of nanoparticles as well as curcumin drug accompany with their MRI analysis, which could affect the MRI signal intensity. Moreover, when folic acid moieties were conjugated to the SiO<sub>2</sub>@HPG and HPG, the hydrophilicity of these nanoparticles also increased, leading to the elevation of their circulation time. Since particles with an  $r_2$  value of more than 20 mM<sup>-1</sup>S<sup>-1</sup> are well suited for the MRI contrast agent, Fe<sub>3</sub>O<sub>4</sub>@SiO<sub>2</sub>@HPG-FA with an  $r_2$  value above 23 mM<sup>-1</sup>S<sup>-1</sup>, compared to non-targeting nanoparticles, possess more potential to be employed as contrast agents in MRI analysis.

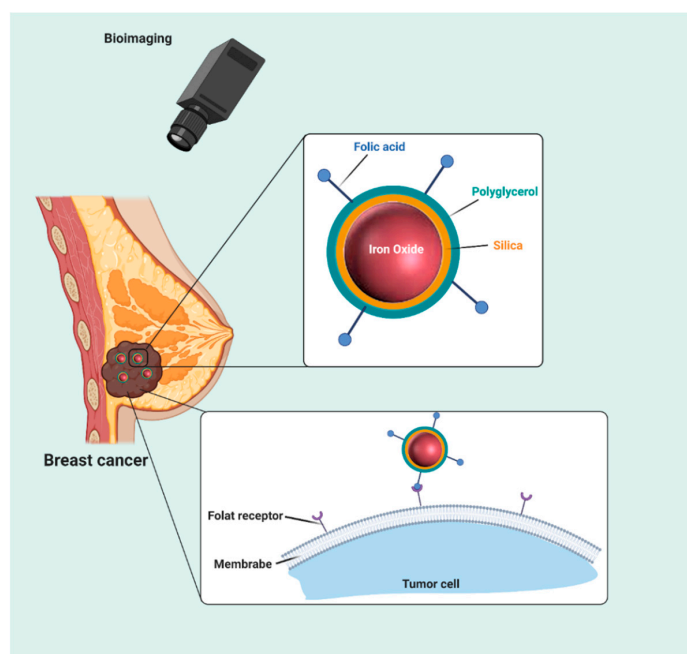


**Figure 9.** Schematic representation of using nanoparticles for selective targeting of breast cancer cells.

## 4. Materials and Methods

### 4.1. Materials

Iron (III) acetylacetonate ( $\text{Fe}(\text{acac})_3$ ), ethyl acetate, dicyclohexylcarbodiimide (DCC), and dimethyl aminopyridine (DMAP) were bought from Merck Co. (Munich, Germany). Triethylene glycol (TREG) was obtained from Novachem (Calgary, Canada). Glycidol, dimethyl sulfoxide (DMSO), tetraethyl orthosilicate (TEOS), (3-Aminopropyl) triethoxysilane (APTES) and folic acid were bought from Sigma Aldrich Co. (St. Louis, MO, USA). For cell culture, the MCF7 cell line was obtained from Pasteur Institute (Tehran, Iran). Dulbecco's modified Eagle's medium (DMEM), phosphate buffer saline (PBS), and penicillin-streptomycin were purchased from BioLidia (Tehran, Iran), and fetal bovine serum (FBS) was obtained from Gibco Co. (Grand Island, NY, USA). 3-(4,5-dimethylthiazol-2)-2,5-diphenyltetrazolium bromide (MTT) was bought from Sigma Co. (Steinheim, Germany).

### 4.2. Fabrication of $\text{Fe}_3\text{O}_4$ Nanoparticles

$\text{Fe}_3\text{O}_4$  nanoparticles were prepared using the polyol method based on previous reports [61]. In summary, 0.053 g of  $\text{Fe}(\text{acac})_3$  and 30 mL TREG were mixed using magnetic stirring. Then, the solution was slowly heated to 300 °C under  $\text{N}_2$  atmosphere, and it was kept at the reflux temperature for about 60 min. After cooling it to room temperature, 20 mL ethyl acetate was added to it while mixing the solution with a shaker. Then, nanoparticles were precipitated through a neodymium magnet and were washed with ethyl acetate three times, and the final precipitate was dried with a freeze-dryer (Vaco 5-ZIRBUS Tech, Harz, Germany) [62].

### 4.3. Synthesis of Polyglycerol Grafted $\text{Fe}_3\text{O}_4$

The anionic ring-opening polymerization of glycidol was carried out in accordance with the literature [33,62,63]. In brief, 1 mL of glycidol monomers was added to 30 mg  $\text{Fe}_3\text{O}_4$  nanoparticles, and the mixture was sonicated at 25 °C for one h before being heated at 140 °C under  $\text{N}_2$  atmosphere for about 20 h. Then, it was cooled to room temperature, the blackish gel was poured into 10 mL DI water, and it was sonicated for 30 min. After dialysis, and the solution against DI-water (dialysis membrane 12 kDa) for 24 h, the nanoparticles were dried by freeze-dryer.

### 4.4. Fabrication of $\text{Fe}_3\text{O}_4$ -Silica Core-Shell Nanoparticles

For other types of nanoparticles,  $\text{Fe}_3\text{O}_4$  nanoparticles were coated by silica at first, and the silica-coated nanoparticles were functionalized by HPG. Briefly, the as-prepared  $\text{Fe}_3\text{O}_4$  nanoparticles suspension was diluted with 60 mL of absolute ethanol with the help of sonication for 15 min, followed by the addition of 30 mL DI water and 25 mL  $\text{NH}_4\text{OH}$  28%. Then, 2 mL tetraethyl orthosilicate (TEOS) was added, and the mixture was handled by sonication at 40 °C for 5 h. The resulting product was collected by an external magnetic field prior to being washed with ethanol several times, with DI water, and acetone, and it was dried with a freeze-dryer. In the next step, 200 mg of  $\text{Fe}_3\text{O}_4$ - $\text{SiO}_2$  was mixed with (3-Aminopropyl) triethoxysilane (APTES) (2 mL); then, the mixture was refluxed in dry toluene (100 mL) at 70 °C for 24 h, and the obtained amino-functionalized MNPs were isolated from the reaction mixture with a permanent external magnet before being washed with ethanol and DI-water several times; then, they were dried with a freeze-dryer [34,35].

### 4.5. Synthesis of $\text{SPION@SiO}_2\text{@HPG}$

First, 100 mg of silica-coated magnetic nanoparticles were dispersed in 2 mL of a saturated potassium methoxide solution in methanol using bath sonication for 30 min, and the solution was stirred at room temperature for one h and refluxed at 80 °C for 2 h. In the end, the magnetic nanoparticles were separated with a magnet, washed with dry methanol three times, and dried with a

freeze-dryer. Then, 2 mL glycidol was added to these deprotonated nanoparticles drop-wise for 15 min at 100 °C, and this mixture was refluxed at this temperature for four h. Then, it was cooled, and the contents were dissolved in methanol. Consequently, the product was separated with a magnet prior to being washed with methanol under sonication several times. The obtained product was dried with a freeze-dryer overnight in order to obtain the HPG-grafted silica-magnetic nanoparticles [42].

#### 4.6. Folic Acid-Targeting of Nanoparticles

Conjugation of folic acid on  $\text{Fe}_3\text{O}_4\text{@HPG}$  and  $\text{Fe}_3\text{O}_4\text{@SiO}_2\text{@HPG}$  was done according to the previous report [45]. Briefly, 5 mg FA and 100 mg  $\text{Fe}_3\text{O}_4$  coated nanoparticles were added to 5 mL dry DMSO, and the mixture was sonicated for 2 min. Subsequently, 1.53 mg DMAP and 2.96 mg DCC were added to this mixture as intermediator. The resulting brown suspension was bath sonicated for 2 min and stirred at 50 °C for 36 h by magnetic stirring. After completing the process, the solution was dialyzed against DI-water (dialysis membrane 12–14 kDa) to remove DMAP, DCC, and unbounded FA. Finally, the solution was dried with a freeze-drier (Figure 10).

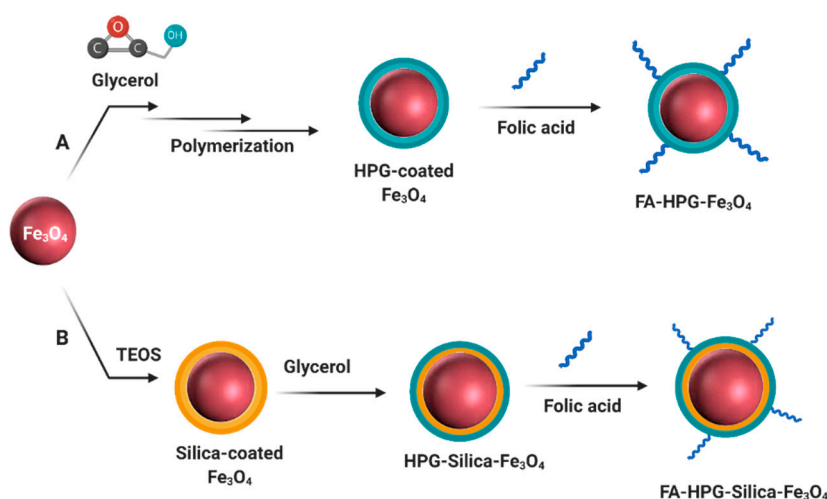


**Figure 10.** Synthesis and preparation of folic acid decorated nanoparticles.

#### 4.7. Characterization Techniques

FT-IR spectra were obtained in a transmission mode (JASCO, FT-IR-6300 (400–4000  $\text{cm}^{-1}$ ), Tsukuba, Japan) to determine the surface modification of nanoparticles. The size and core-shell structure of nanoparticles were observed with transmission electron microscopy (JEOL JEM-ARM200CFEG UHR-TEM (Peabody, MA, USA) (equipped with STEM, Cs corrected STEM, EDS, Gatan Quantum GIF and Digital CCD Camera)). Magnetization measurements were carried out on a certain amount of ferrofluid by employing a vibrating sample magnetometer (VSM; MDKFT, Kosar Kashan Magnetics Corporation, IR, Kashan, Iran). This system specifies the amount and magnetization behavior of the sample as a function of the changes in the intensity of the constant magnetic field applied.

#### 4.8. MTT Assay

The cytotoxicity of nanoparticles was determined using the MTT colorimetric assay. In this test, MCF-7 cell line, as a type of cancer cell with overexpression of FA receptor, was seeded in 96-well plates at a density of 5000 cells/well in 100  $\mu\text{L}$  of medium, and it was incubated overnight at 37 °C in 5%  $\text{CO}_2$ . After 24 h of incubation, the media of all wells were replaced with 100  $\mu\text{L}$  of fresh media, holding different concentrations (25, 50, 100, and 200  $\mu\text{g}/\text{mL}$ ) of nanoparticles. All concentrations were replicated in three wells. After 24 and 48 h of incubation, the media were removed, and cells were washed with PBS twice. Then, 100  $\mu\text{L}$  of pure medium was added to each well, followed by the addition of 10  $\mu\text{L}$  of MTT solution (5  $\text{mg}/\text{mL}$  in PBS), and the plates were incubated for four h at 37 °C.

Then, the media were replaced by 100  $\mu$ L DMSO and the plates were incubated for another 1 h. Finally, the wells absorbance was measured at 490 nm with a microplate reader (Bio-Rad Laboratories, Inc., Hercules, CA, USA), in order to determine the viability of the cells.

#### 4.9. In Vitro MR Imaging

MR imaging was carried out with a clinical 1.5 T MR Imager and a high-resolution head coil. MCF-7 cell line (250,000 cells per well) was incubated with different concentrations of SPION@HPG, SPION@HPG-FA, SPION@SiO<sub>2</sub>@HPG and SPION@SiO<sub>2</sub>@HPG-FA (0.0625, 0.125, 0.250 and 0.500 mM Fe) for 4 h. Then, the cells were washed with PBS twice to remove non-attached nanoparticles. The attached cells were then separated by adding trypsin and re-suspending in 1.5 mL gelatin. Determination of the  $T_2$  relaxation times was carried out by a multi-echo spine-echo sequence (repetition time (TR): 3000 ms; echo time (TE): 18–144 ms), slice thickness of 20 mm, and the field of view of 160 mm. The relaxation times for each sample were calculated by using in-house software (MATLAB 2016b) by non-linear least-squares fitting of appropriate exponential functions. Transverse relativities ( $r_2$ ) were calculated as the slope of the lines fitted by linear regression analysis (Microsoft EXCEL) to relaxation rates ( $1/T_2$ ).

## 5. Conclusions

In this research, the coating and targeting of iron oxide nanoparticles were compared and evaluated on their relaxivity, by conjugating HPG and SiO<sub>2</sub>@HPG as coating agents and the FA ligand as a targeting agent on the surface of nanoparticles. The findings of the research revealed that the amount of magnetic saturation for SiO<sub>2</sub>@HPG coating nanoparticles was higher than HPG coating. SiO<sub>2</sub>@HPG-FA targeted nanoparticles showed a high relaxivity of 23.25 mM<sup>-1</sup>S<sup>-1</sup> compared to non-targeted SiO<sub>2</sub>@HPG nanoparticles. Moreover, HPG targeted nanoparticles have an  $r_2$  value of about 0.131 mM<sup>-1</sup>S<sup>-1</sup>—considerably lower than SiO<sub>2</sub>@HPG@FA nanoparticles. Therefore, FA ligand could award this nanoparticle with targeting specificity to the tumor cells via receptor-mediated endocytosis. With these promising properties, Fe<sub>3</sub>O<sub>4</sub>@SiO<sub>2</sub>@HPG-FA nanoparticles have good potential to be used as MRI contrast agents in cells that have over-expression of folate receptors. However, future studies should be devoted to carry out in vivo test to understand its potential bio-applications.

**Author Contributions:** Conceptualization: A.Z. (Ali Zarrabi), I.J. and A.T.; Methodology: A.Z. (Atefeh Zarepour), H.H.S.H. and M.A.; Preparing first draft: M.A., H.H.S.H. and A.Z. (Atefeh Zarepour); Critical editing of manuscript: A.Z. (Ali Zarrabi) and P.M. All authors have read and agreed to the published version of the manuscript.

**Funding:** This research received no external funding.

**Conflicts of Interest:** The authors declare no conflict of interest.

## References

1. Mohammadinejad, R.; Dehshahri, A.; Sagar Madamsetty, V.; Zahmatkeshan, M.; Tavakol, S.; Makvandi, P.; Khorsandi, D.; Pardakhty, A.; Ashrafizadeh, M.; Ghasemipour Afshar, E.; et al. In vivo gene delivery mediated by non-viral vectors for cancer therapy. *J. Control. Release* **2020**, *325*, 249–275. [[CrossRef](#)]
2. Makvandi, P.; Ghomi, M.; Padil, V.V.T.; Shalchy, F.; Ashrafizadeh, M.; Askarinejad, S.; Pourreza, N.; Zarrabi, A.; Nazarzadeh Zare, E.; Kooti, M.; et al. Biofabricated Nanostructures and Their Composites in Regenerative Medicine. *ACS Appl. Nano Mater.* **2020**, *3*, 6210–6238. [[CrossRef](#)]
3. Wang, C.; Makvandi, P.; Zare, E.N.; Tay, F.R.; Niu, L. Advances in Antimicrobial Organic and Inorganic Nanocompounds in Biomedicine. *Adv. Ther.* **2020**, *3*, 2000024. [[CrossRef](#)]
4. George, J.M.; Antony, A.; Mathew, B. Metal oxide nanoparticles in electrochemical sensing and biosensing: A review. *Microchim. Acta* **2018**, *185*, 358. [[CrossRef](#)] [[PubMed](#)]
5. Mukherjee, S.; Madamsetty, V.S.; Bhattacharya, D.; Roy Chowdhury, S.; Paul, M.K.; Mukherjee, A. Recent advancements of nanomedicine in neurodegenerative disorders theranostics. *Adv. Funct. Mater.* **2020**, 2003054. [[CrossRef](#)]

6. Leng, F.; Liu, F.; Yang, Y.; Wu, Y.; Tian, W. Strategies on nanodiagnostics and nanotherapies of the three common cancers. *Nanomaterials* **2018**, *8*, 202. [[CrossRef](#)] [[PubMed](#)]
7. Vallabani, N.V.S.; Singh, S.; Karakoti, A. Magnetic nanoparticles: Current trends and future aspects in diagnostics and nanomedicine. *Curr. Drug Metab.* **2019**, *20*, 457–472. [[CrossRef](#)]
8. Hashemi, R.H.; Bradley, W.G.; Lisanti, C.J. *MRI: The Basics*; Lippincott Williams & Wilkins: Philadelphia, PA, USA, 2012; ISBN 1451148712.
9. Issa, B.; Obaidat, I.M. Magnetic nanoparticles as MRI contrast agents. In *Magnetic Resonance Imaging*; IntechOpen: London, UK, 2019.
10. Tocchio, S.; Kline-Fath, B.; Kanal, E.; Schmithorst, V.J.; Panigrahy, A. MRI evaluation and safety in the developing brain. *Semin. Perinatol.* **2015**, *39*, 73–104. [[CrossRef](#)]
11. Lee, N.; Yoo, D.; Ling, D.; Cho, M.H.; Hyeon, T.; Cheon, J. Iron oxide based nanoparticles for multimodal imaging and magnetoresponsive therapy. *Chem. Rev.* **2015**, *115*, 10637–10689. [[CrossRef](#)]
12. Zhao, X.; Zhao, H.; Chen, Z.; Lan, M. Ultrasmall superparamagnetic iron oxide nanoparticles for magnetic resonance imaging contrast agent. *J. Nanosci. Nanotechnol.* **2014**, *14*, 210–220. [[CrossRef](#)]
13. Mahmoudi, M.; Serpooshan, V.; Laurent, S. Engineered nanoparticles for biomolecular imaging. *Nanoscale* **2011**, *3*, 3007–3026. [[CrossRef](#)] [[PubMed](#)]
14. Na, H.B.; Song, I.C.; Hyeon, T. Inorganic nanoparticles for MRI contrast agents. *Adv. Mater.* **2009**, *21*, 2133–2148. [[CrossRef](#)]
15. Qiao, R.; Yang, C.; Gao, M. Superparamagnetic iron oxide nanoparticles: From preparations to in vivo MRI applications. *J. Mater. Chem.* **2009**, *19*, 6274–6293. [[CrossRef](#)]
16. Arsalani, N.; Fattahi, H.; Laurent, S.; Burtea, C.; Elst, L.V.; Muller, R.N. Polyglycerol-grafted superparamagnetic iron oxide nanoparticles: Highly efficient MRI contrast agent for liver and kidney imaging and potential scaffold for cellular and molecular imaging. *Contrast Media Mol. Imaging* **2012**, *7*, 185–194. [[CrossRef](#)]
17. Reddy, L.H.; Arias, J.L.; Nicolas, J.; Couvreur, P. Magnetic nanoparticles: Design and characterization, toxicity and biocompatibility, pharmaceutical and biomedical applications. *Chem. Rev.* **2012**, *112*, 5818–5878. [[CrossRef](#)]
18. Bigall, N.C.; Dilena, E.; Dorfs, D.; Beoutis, M.-L.; Pugliese, G.; Wilhelm, C.; Gazeau, F.; Khan, A.A.; Bittner, A.M.; Garcia, M.A. Hollow iron oxide nanoparticles in polymer nanobeads as MRI contrast agents. *J. Phys. Chem. C* **2015**, *119*, 6246–6253. [[CrossRef](#)]
19. Albinali, K.E.; Zagho, M.M.; Deng, Y.; Elzatahry, A.A. A perspective on magnetic core-shell carriers for responsive and targeted drug delivery systems. *Int. J. Nanomed.* **2019**, *14*, 1707. [[CrossRef](#)]
20. Wang, L.; Neoh, K.G.; Kang, E.-T.; Shuter, B. Multifunctional polyglycerol-grafted Fe<sub>3</sub>O<sub>4</sub>@SiO<sub>2</sub> nanoparticles for targeting ovarian cancer cells. *Biomaterials* **2011**, *32*, 2166–2173. [[CrossRef](#)]
21. Wang, L.; Neoh, K.G.; Kang, E.T.; Shuter, B.; Wang, S. Superparamagnetic hyperbranched polyglycerol-grafted Fe<sub>3</sub>O<sub>4</sub> nanoparticles as a novel magnetic resonance imaging contrast agent: An in vitro assessment. *Adv. Funct. Mater.* **2009**, *19*, 2615–2622. [[CrossRef](#)]
22. Das, P.; Jana, N.R. Highly colloidally stable hyperbranched polyglycerol grafted red fluorescent silicon nanoparticle as bioimaging probe. *ACS Appl. Mater. Interfaces* **2014**, *6*, 4301–4309. [[CrossRef](#)]
23. Moore, E.; Delalat, B.; Vasani, R.; McPhee, G.; Thissen, H.; Voelcker, N.H. Surface-initiated hyperbranched polyglycerol as an ultralow-fouling coating on glass, silicon, and porous silicon substrates. *ACS Appl. Mater. Interfaces* **2014**, *6*, 15243–15252. [[CrossRef](#)] [[PubMed](#)]
24. Mahmoudi, M.; Sant, S.; Wang, B.; Laurent, S.; Sen, T. Superparamagnetic iron oxide nanoparticles (SPIONs): development, surface modification and applications in chemotherapy. *Adv. Drug Deliv. Rev.* **2011**, *63*, 24–46. [[CrossRef](#)] [[PubMed](#)]
25. Yuan, P.; Ding, X.; Yang, Y.Y.; Xu, Q. Metal nanoparticles for diagnosis and therapy of bacterial infection. *Adv. Healthc. Mater.* **2018**, *7*, 1701392. [[CrossRef](#)] [[PubMed](#)]
26. Kim, J.-E.; Shin, J.-Y.; Cho, M.-H. Magnetic nanoparticles: an update of application for drug delivery and possible toxic effects. *Arch. Toxicol.* **2012**, *86*, 685–700. [[CrossRef](#)] [[PubMed](#)]
27. Laurent, S.; Forge, D.; Port, M.; Roch, A.; Robic, C.; Vander-Elst, L.; Muller, R.N. Magnetic iron oxide nanoparticles: synthesis, stabilization, vectorization, physicochemical characterizations, and biological applications. *Chem. Rev.* **2008**, *108*, 2064–2110. [[CrossRef](#)] [[PubMed](#)]

28. Amin, N.; Araj, S. Morin temperature of annealed submicronic  $\alpha$ - $\text{Fe}_2\text{O}_3$  particles. *Phys. Rev. B* **1987**, *35*, 4810. [[CrossRef](#)]
29. Ortega, G.; Reguera, E. Biomedical applications of magnetite nanoparticles. In *Materials for Biomedical Engineering*; Elsevier: Amsterdam, The Netherlands, 2019; pp. 391–428.
30. Chowdhuri, A.R.; Bhattacharya, D.; Sahu, S.K. Magnetic nanoscale metal organic frameworks for potential targeted anticancer drug delivery, imaging and as an MRI contrast agent. *Dalton Trans.* **2016**, *45*, 2963–2973. [[CrossRef](#)]
31. Li, L.; Gao, F.; Jiang, W.; Wu, X.; Cai, Y.; Tang, J.; Gao, X.; Gao, F. Folic acid-conjugated superparamagnetic iron oxide nanoparticles for tumor-targeting MR imaging. *Drug Deliv.* **2016**, *23*, 1726–1733. [[CrossRef](#)]
32. Zhang, Y.; Zhang, T.; Liu, M.; Kuang, Y.; Zu, G.; Zhang, K.; Cao, Y.; Pei, R. Aptamer-targeted magnetic resonance imaging contrast agents and their applications. *J. Nanosci. Nanotechnol.* **2018**, *18*, 3759–3774. [[CrossRef](#)]
33. Mousavi, H.; Movahedi, B.; Zarrabi, A.; Jahandar, M. A multifunctional hierarchically assembled magnetic nanostructure towards cancer nano-theranostics. *RSC Adv.* **2015**, *5*, 77255–77263. [[CrossRef](#)]
34. Toriki, M.; Tangestaninejad, S.; Mirkhani, V.; Moghadam, M.; Mohammadpoor-Baltork, I. Ru(III) Salophen- $\text{CH}_2$ - $\text{NH}_2$ - $\text{SiO}_2$ -Fe: An efficient and magnetically recoverable catalyst for trimethylsilylation of alcohols and phenols with hexamethyldisilazane. *Appl. Organomet. Chem.* **2014**, *28*, 304–309. [[CrossRef](#)]
35. Shahrestani, H.; Taheri-Kafrani, A.; Soozanipour, A.; Tavakoli, O. Enzymatic clarification of fruit juices using xylanase immobilized on 1, 3, 5-triazine-functionalized silica-encapsulated magnetic nanoparticles. *Biochem. Eng. J.* **2016**, *109*, 51–58. [[CrossRef](#)]
36. Dadfar, S.M.; Roemhild, K.; Drude, N.I.; von Stillfried, S.; Knüchel, R.; Kiessling, F.; Lammers, T. Iron oxide nanoparticles: Diagnostic, therapeutic and theranostic applications. *Adv. Drug Deliv. Rev.* **2019**, *138*, 302–325. [[CrossRef](#)] [[PubMed](#)]
37. Yu, M.K.; Park, J.; Jon, S. Targeting strategies for multifunctional nanoparticles in cancer imaging and therapy. *Theranostics* **2012**, *2*, 3. [[CrossRef](#)] [[PubMed](#)]
38. Nordmeyer, D.; Stumpf, P.; Gröger, D.; Hofmann, A.; Enders, S.; Riese, S.B.; Dervede, J.; Taupitz, M.; Rauch, U.; Haag, R. Iron oxide nanoparticles stabilized with dendritic polyglycerols as selective MRI contrast agents. *Nanoscale* **2014**, *6*, 9646–9654. [[CrossRef](#)] [[PubMed](#)]
39. Yang, X.; Wen, Y.; Wu, A.; Xu, M.; Amano, T.; Zheng, L.; Zhao, L. Polyglycerol mediated covalent construction of magnetic mesoporous silica nanohybrid with aqueous dispersibility for drug delivery. *Mater. Sci. Eng. C* **2017**, *80*, 517–525. [[CrossRef](#)]
40. Makvandi, P.; Ali, G.W.; Della Sala, F.; Abdel-Fattah, W.I.; Borzacchiello, A. Biosynthesis and characterization of antibacterial thermosensitive hydrogels based on corn silk extract, hyaluronic acid and nanosilver for potential wound healing. *Carbohydr. Polym.* **2019**, *223*, 115023. [[CrossRef](#)]
41. Makvandi, P.; Ali, G.W.; Della Sala, F.; Abdel-Fattah, W.I.; Borzacchiello, A. Hyaluronic acid/corn silk extract based injectable nanocomposite: A biomimetic antibacterial scaffold for bone tissue regeneration. *Mater. Sci. Eng. C* **2019**, *107*, 10195. [[CrossRef](#)]
42. Landarani-Isfahani, A.; Taheri-Kafrani, A.; Amini, M.; Mirkhani, V.; Moghadam, M.; Soozanipour, A.; Razmjou, A. Xylanase immobilized on novel multifunctional hyperbranched polyglycerol-grafted magnetic nanoparticles: an efficient and robust biocatalyst. *Langmuir* **2015**, *31*, 9219–9227. [[CrossRef](#)]
43. Mu, S.; Li, G.; Liang, Y.; Wu, T.; Ma, D. Hyperbranched polyglycerol-modified graphene oxide as an efficient drug carrier with good biocompatibility. *Mater. Sci. Eng. C* **2017**, *78*, 639–646. [[CrossRef](#)]
44. Khelghati, N.; Rasmi, Y.; Farahmandan, N.; Sadeghpour, A.; Mir, S.M.; Karimian, A.; Yousefi, B. Hyperbranched polyglycerol  $\beta$ -cyclodextrin as magnetic platform for optimization of doxorubicin cytotoxic effects on Saos-2 bone cancerous cell line. *J. Drug Deliv. Sci. Technol.* **2020**, *57*, 101741. [[CrossRef](#)]
45. Mostaghassi, E.; Zarepour, A.; Zarrabi, A. Folic acid armed  $\text{Fe}_3\text{O}_4$ -HPG nanoparticles as a safe nano vehicle for biomedical theranostics. *J. Taiwan Inst. Chem. Eng.* **2018**, *82*, 33–41. [[CrossRef](#)]
46. Sun, C.; Sze, R.; Zhang, M. Folic acid-PEG conjugated superparamagnetic nanoparticles for targeted cellular uptake and detection by MRI. *J. Biomed. Mater. Res. Part A* **2006**, *78*, 550–557. [[CrossRef](#)] [[PubMed](#)]
47. Cao, W.; Wang, X.; Song, L.; Wang, P.; Hou, X.; Zhang, H.; Tian, X.; Liu, X.; Zhang, Y. Folic acid-conjugated gold nanorod@ polypyrrole@  $\text{Fe}_3\text{O}_4$  nanocomposites for targeted MR/CT/PA multimodal imaging and chemo-photothermal therapy. *RSC Adv.* **2019**, *9*, 18874–18887. [[CrossRef](#)]

48. Vallabani, N.V.S.; Singh, S. Recent advances and future prospects of iron oxide nanoparticles in biomedicine and diagnostics. *3 Biotech* **2018**, *8*, 279. [[CrossRef](#)] [[PubMed](#)]
49. Bao, Y.; Sherwood, J.A.; Sun, Z. Magnetic iron oxide nanoparticles as T 1 contrast agents for magnetic resonance imaging. *J. Mater. Chem. C* **2018**, *6*, 1280–1290. [[CrossRef](#)]
50. Lao, C.S.; Liu, J.; Gao, P.; Zhang, L.; Davidovic, D.; Tummala, R.; Wang, Z.L. ZnO nanobelt/nanowire Schottky diodes formed by dielectrophoresis alignment across Au electrodes. *Nano Lett.* **2006**, *6*, 263–266. [[CrossRef](#)]
51. Hobson, N.J.; Weng, X.; Siow, B.; Veiga, C.; Ashford, M.; Thanh, N.T.K.; Schätzlein, A.G.; Uchegbu, I.F. Clustering superparamagnetic iron oxide nanoparticles produces organ-targeted high-contrast magnetic resonance images. *Nanomedicine* **2019**, *14*, 1135–1152. [[CrossRef](#)]
52. Ghasemi, A.; Jafari, S.; Salehi, I. Synthesis and characterization of polyglycerol coated superparamagnetic iron oxide nanoparticles and cytotoxicity evaluation on normal human cell lines. *Colloids Surf. A Physicochem. Eng. Asp.* **2018**, *551*, 128–136. [[CrossRef](#)]
53. Marín, T.; Montoya, P.; Arnache, O.; Calderón, J. Influence of surface treatment on magnetic properties of Fe<sub>3</sub>O<sub>4</sub> nanoparticles synthesized by electrochemical method. *J. Phys. Chem. B* **2016**, *120*, 6634–6645. [[CrossRef](#)]
54. Palomec-Garfias, A.F.; Jardim, K.V.; Sousa, M.H.; Márquez-Beltrán, C. Influence of polyelectrolyte chains on surface charge and magnetization of iron oxide nanostructures. *Colloids Surf. A Physicochem. Eng. Asp.* **2018**, *549*, 13–24. [[CrossRef](#)]
55. Hajesmaelzadeh, F.; Shanehsazzadeh, S.; Grüttner, C.; Daha, F.J.; Oghabian, M.A. Effect of coating thickness of iron oxide nanoparticles on their relaxivity in the MRI. *Iran. J. Basic Med. Sci.* **2016**, *19*, 166. [[PubMed](#)]
56. Bitar, A.; Ahmad, N.M.; Fessi, H.; Elaissari, A. Silica-based nanoparticles for biomedical applications. *Drug Discov. Today* **2012**, *17*, 1147–1154. [[CrossRef](#)]
57. Muhamad, N.; Plengsuriyakarn, T.; Na-Bangchang, K. Application of active targeting nanoparticle delivery system for chemotherapeutic drugs and traditional/herbal medicines in cancer therapy: A systematic review. *Int. J. Nanomed.* **2018**, *13*, 3921. [[CrossRef](#)] [[PubMed](#)]
58. Zhang, H.; Li, J.; Hu, Y.; Shen, M.; Shi, X.; Zhang, G. Folic acid-targeted iron oxide nanoparticles as contrast agents for magnetic resonance imaging of human ovarian cancer. *J. Ovarian Res.* **2016**, *9*, 19. [[CrossRef](#)]
59. Kevadiya, B.D.; Bade, A.N.; Woldstad, C.; Edagwa, B.J.; McMillan, J.M.; Sajja, B.R.; Boska, M.D.; Gendelman, H.E. Development of europium doped core-shell silica cobalt ferrite functionalized nanoparticles for magnetic resonance imaging. *Acta Biomater.* **2017**, *49*, 507–520. [[CrossRef](#)] [[PubMed](#)]
60. Gholibegloo, E.; Mortezaadeh, T.; Salehian, F.; Forootanfar, H.; Firoozpour, L.; Foroumadi, A.; Ramazani, A.; Khoobi, M. Folic acid decorated magnetic nanosponge: An efficient nanosystem for targeted curcumin delivery and magnetic resonance imaging. *J. Colloid Interface Sci.* **2019**, *556*, 128–139. [[CrossRef](#)] [[PubMed](#)]
61. Yang, W.J.; Lee, J.H.; Hong, S.C.; Lee, J.; Lee, J.; Han, D.-W. Difference between toxicities of iron oxide magnetic nanoparticles with various surface-functional groups against human normal fibroblasts and fibrosarcoma cells. *Materials* **2013**, *6*, 4689–4706. [[CrossRef](#)]
62. Zhao, L.; Chano, T.; Morikawa, S.; Saito, Y.; Shiino, A.; Shimizu, S.; Maeda, T.; Irie, T.; Aonuma, S.; Okabe, H. Hyperbranched polyglycerol-grafted superparamagnetic iron oxide nanoparticles: Synthesis, characterization, functionalization, size separation, magnetic properties, and biological applications. *Adv. Funct. Mater.* **2012**, *22*, 5107–5117. [[CrossRef](#)]
63. Jahandar, M.; Zarrabi, A.; Shokrgozar, M.A.; Mousavi, H. Synthesis, characterization and application of polyglycerol coated Fe<sub>3</sub>O<sub>4</sub> nanoparticles as a nano-theranostics agent. *Mater. Res. Express* **2015**, *2*, 125002. [[CrossRef](#)]

**Sample Availability:** Samples of the modified iron oxide are available from the authors.



© 2020 by the authors. Licensee MDPI, Basel, Switzerland. This article is an open access article distributed under the terms and conditions of the Creative Commons Attribution (CC BY) license (<http://creativecommons.org/licenses/by/4.0/>).